Stokes dual-soliton spectroscopy in a graphene functionalized over-modal microresonator

Giancarlo Soavi (✉ giancarlo.soavi@uni-jena.de)
Friedrich Schiller University Jena   https://orcid.org/0000-0003-2434-2251

Zhongye Yuan
University of Electronic Science and Technology of China

Teng Tan
University of Electronic Science and Technology of China

Guofeng Yan
Zhejiang Laboratory

Siyu Zhou
University of Electronic Science and Technology of China

Ning An
University of Electronic Science and Technology of China

Hao Zhang
University of Electronic Science and Technology of China

Bo Peng
University of Electronic Science and Technology of China   https://orcid.org/0000-0001-9411-716X

Yun-Jiang Rao
University of Electronic Science and Technology of China

Baicheng Yao
University of Electronic Science and Technology of China   https://orcid.org/0000-0001-8368-5815

Abstract

Dual comb spectroscopy enables fast and accurate measurements over broad spectral ranges, offering a powerful tool to identify chemical species with unprecedented spectral resolution. Co-generation of soliton combs in one single microresonator can be used to improve the compactness of multi-comb sources and bridge the lab-to-fab gap. However, the robustness of pristine microresonators to environmental changes limits their potential in broader applications such as biochemical sensing. Here, we realize for the first time a two-dimensional-material functionalized dual-comb spectrometer by asymmetrically depositing graphene in an over-modal microsphere. Spectrally trapped Stokes solitons belonging to distinct transverse mode families are co-generated in one single device. A soliton mode in the graphene-functionalized region is highly sensitive to environmental changes while a second soliton mode in the pristine region serves as reference, thus producing dual-comb ultrasensitive beat notes in the electrical domain. Taking advantage of an advanced optoelectronic heterodyne detection scheme, we trace the frequency shift of the dual-soliton beat-note with uncertainty < 0.2 Hz and we achieve real-time individual gas molecule detection in vacuum. This combination of atomically thin materials and microcombs shows the potential for integrated spectroscopy with unprecedented performances and offers new insights toward the design of versatile functionalized microcavity photonic devices.

Main Text

Achieving ultra-high sensitivity is one of the major goals and challenges of any detection scheme. In the case of chemical sensors aiming at single molecule detection, advanced schemes based on the measurement of the photothermal shift [11], the evanescent wave amplitude in nanowires [12], the plasmonically enhanced scattering [13,14], fluorescent behaviors [9,15] and the mode splitting at the exceptional point [16,17] have been proposed. However, detection of individual gas molecules using integrated photonic devices is still a challenge because of the stringent requirements in terms of spectral resolution and ultralow noise. Dual-comb spectroscopy based on Kerr or Raman solitons [18] naturally has narrow linewidth and high frequency stability and could thus be the ideal tool to achieve individual molecule detection on microscale photonic devices and on-chip. However, the inert nature of the materials (silica, silicon nitride or metal fluorides) that are typically used for soliton microcomb devices inhibits gas adsorption and sensing applications. In this context, chemical functionalization could significantly expand the capability of dual-comb devices for sensing applications. Here we demonstrate that functionalization of an over-modal microresonator with a single layer of graphene allows to realize a dual-comb spectrometer with unprecedented chemically sensitivity. Leveraging such graphene functionalized dual-comb microresonator, we successfully achieve individual gas molecule detection at high-speed. Such graphene-microcavity device, which has been used for optoelectronic tuning of frequency comb generation [19,20,21,22], was never used in comb spectroscopy to date. Our results stem from the precise spatial positioning of the graphene flake on the microcavity to create a unique 'reference-probe' dual-comb system. In particular, by depositing graphene 30º away from the equator of the microcavity we generate one Stokes soliton interacting with graphene (probe) and one Stokes soliton

from the pristine microcavity (reference). Molecule adsorption on graphene changes its Fermi level [19,23] and thus modifies the free-spectrum-range of the probe comb. Finally, taking advantage of an advanced optoelectronic heterodyne detection scheme, we trace the frequency shift of the dual-soliton beat-note with uncertainty < 0.2 Hz to detect single molecule dynamics.

Fig. 1a shows the conceptual design of the graphene based micro dual-comb device (GMDC). A silica microsphere with diameter $\approx$ 600 μm and typical intrinsic Q factor $\approx$ 3×10^8 is used for the Kerr and Stokes soliton generation. Thanks to its large mode volume, such a microsphere supports multiple transverse co-oscillating intracavity modes, driven by one single pump laser. This enables different soliton frequencies to be generated simultaneously either in a low-order mode (blue arrow) or in a high-order mode (yellow). In this architecture, a mechanically exfoliated graphene flake is deposited on the surface of the microsphere by deterministic dry-transfer [24]. The position of graphene is carefully controlled to be 30° above the equatorial plane, to ensure the overlap only with the high order modes (with wider energy distribution) of the microcavity. On the other hand, the fundamental mode, which distributes tightly along the equator, will not be affected by the presence of graphene. Such scheme will provide both the "probe" (graphene functionalized) and "reference" (pristine) combs, as we show in the following. Moreover, positioning the graphene away from the equator also prevents its damage and heating when the intracavity power is high (up to tens of watts). **Fig. 1b** shows a top-view optical microscopy picture of our device and a scanning electron microscopy image where the atomically smooth surface of the silica microresonator and the 80 × 30 μm^2 graphene layer are clearly visible. More details about the transfer method and characterization of the device are available in the Supplementary Notes S3 & S4.

Fig. 1c illustrates the measured intracavity intensity evolution of the Kerr and Stokes combs, which are traced synchronously by using a C+L/U band wavelength division multiplexer. When red scanning the pump laser (at fixed power 200 mW) from 1549 nm to 1550 nm with a scanning speed of 500 MHz/ms, a Kerr comb begins to form and creates Raman amplification. To observe both Kerr and Stokes solitons, the following four conditions must be satisfied: 1) the Stokes soliton lines must lie within the Raman gain spectrum generated by the Kerr soliton; 2) the FSR of the Stokes solitons must be close to that of the Kerr soliton; 3) the mode family of Kerr soliton and Stokes solitons overlap efficiently in both space and time; 4) the pump power reaches the Raman threshold. In this way, the Stokes solitons rely on the existence of the Kerr soliton due to the spatial-temporal overlap for Kerr effect trapping and Raman amplification. In **Fig.1c** one can also observe that the Kerr soliton step appears earlier than the Stokes soliton step. Further theoretical analysis is available in Supplementary Notes S1 and S2. **Fig. 1d** plots the optical spectrum of the co-generated Kerr and Stokes solitons. The Kerr soliton spans from 1500 nm to 1600 nm, while the multiple Stokes solitons are generated in the band from 1650 nm to 1700 nm. Although their central wavelengths are different, the Stokes solitons shows FSRs similar to those of the Kerr soliton. In the zoomed-in panel, we also observe that the excited Stokes solitons have distinct comb envelopes, since they belong to different mode families. This means that one Kerr soliton can trap many Stokes solitons

thanks to the over-modal nature of the microresonator. As a consequence, these Stokes solitons can beat with each other, offering a powerful tool for dual-comb spectroscopy in the electrical domain.

Fig. 2a maps the frequency-resolved auto-correlation traces of the Kerr soliton and the Stokes solitons based on second-harmonic generation (SHG). First, in the C band (1550 nm), the pulse structure with 10.24 ps interval clearly suggests the existence of a single Kerr soliton. Based on the autocorrelation trace, the measured pulse duration of the Kerr soliton is 350 fs, as expected from the 3 dB spectral range of 0.93 THz. On the other hand, in the U band (1670 nm), the signal to noise ratio of the auto-correlation trace is lower because the Stokes solitons contain pulse trains with different repetition rates. These Stokes solitons with different repetition rates can interfere leading to a frequency down-conversion in the radio frequency domain. **Fig. 2b** plots the beating signal of a pair of dual Stokes solitons. This beat note can't be due to the Kerr-Stokes interaction, as they don't overlap in frequency (photon energy). The dual Stokes soliton beating provides an electrical comb with 7.514 MHz spacing, such a frequency difference is more than 4 orders of magnitude smaller than the soliton FSR. (in Supplementary Note S5 we also show that the dual soliton modes with 7.514 MHz FSR difference have orthogonal polarizations.). The zoomed-in panel shows more details on the dual Stokes soliton beating. The signal-to-noise ratio (SNR) of the first beating line is > 55 dB and its spectral linewidth is < 10 Hz. Moreover, **Fig. 2c** shows the measured single-sideband (SSB) phase noise of this beat note and reveals that the phase noise is < -130 dBc/Hz at 10 kHz, and < -140 dBc/Hz at 1 MHz. This result could be further optimized by using active feedback [22,25,26]. In **Fig. 2d**, we measure the long-term stability of the 7.514 MHz beating signal. For a continuous measurement of 2 hours at room temperature the frequency shift is < 2.5 Hz and the intensity variation is < ±0.1 dB. Such a high stability with uncertainty at the Hz level offers a unique platform for gas sensing applications.

Fig. 3a shows a schematic of our gas sensing device for individual molecule detection. In the microresonator, the reference Stokes soliton at the equator has a FSR f_R while the probe Stokes soliton interacting with the graphene flake has a FSR f_P, and their beating down conversion frequency is $\Delta f = f_R - f_P$. Once gas molecules are adsorbed on the graphene flake the refractive index experienced by the probe soliton will change, leading to a change of f_P. As a result, we will detect a shift of the beating frequency Δf, that we can measure in the electrical domain to obtain the gas dynamics with individual molecule sensitivity. **Fig. 3b** explains the optical refractive index change induced by adsorption of individual gas molecules on graphene. The Fermi level of graphene is related to the carrier density by $|E_F| \approx \hbar |v_F|(\pi N)^{-1/2}$ [27], where N is the carrier density, $v_F \approx 10^6$ m/s is the Fermi velocity, and $\hbar$ is the reduced Plank's constant. In this equation, N includes both the intrinsic doping and the external doping, determined in our case by the gas adsorption. Tuning of the Fermi level affects the refractive index of graphene, as explained in details in Refs [19,28] and in the Supplementary Note S6. In the right panels of **Fig. 3b**, we show the calculated real and imaginary refractive index spectra of the graphene ($Re\{n_g\}$ and $Im\{n_g\}$) for different values of the Fermi level and wavelengths in the range 1500 nm – 1700 nm. For our application, at the wavelength ≈ 1670 nm an increment of the Fermi level from 0 eV to 0.31 eV induces a change of the $Re\{n_g\}$ from 2.75 to 3.25, thus approximately 1.61/eV. In this work, we use ammonia (NH_3) molecules

as a sensing target [23,29]. The adsorption of a single NH_3 molecule provides 2 additional electrons to graphene. Considering that the area of the (p-doped) graphene flake is 1.6×10^{-9} m^2, the adsorption of a single NH_3 molecule will induce a $|E_F|$ reduction of 1.7×10^{-4} eV. As a result, $Re\{n_g\}$ will decrease by 2.74×10^{-4} inducing an increase of the probe comb mode FSR and a spectral shift of the reference-probe comb beat note.

Fig. 3c shows the measured shifts of the reference-probe comb beat note for different values of NH_3 concentration in the pM/L range. For this experiment, we put our GMDC device in a vacuum chamber with volume of 8 L (the setup is shown in the Supplementary Note S7) and we inject pure NH_3 gas in the vacuum chamber, controlling the minimum concentration of the NH_3 in steps of 0.5 pM/L. When the NH_3 concentration is 0.5 pM/L, 1 pM/L, 2 pM/L, 4 pM/L, and 8 pM/L, we record dual-comb beat note shifts of 85 Hz, 159 Hz, 203 Hz, 230 Hz, and 248 Hz respectively. **Fig. 3d** summarizes the performances of our sensing device. The maximum sensitivity reaches 170 Hz/(pM/L) in the 0 ~ 0.5 pM/L region, while a higher in-chamber gas concentration gives lower sensitivity due to saturation of the gas adsorption. In repeated measurements, the gas molecules attached on graphene can be > 99% released simply by heating the device via an electrical heater. Moreover, after repeated use the sensitivity of the dual-comb sensor does not deteriorate.

To achieve single molecule detection, we further implement a heterodyne lock-in amplification scheme, as shown schematically in **Fig. 4a**. We use a signal generator to produce a RF line with a stable frequency of 7.464 MHz to beat the 7.514 MHz signal (Δf), thus forming a new 50 kHz frequency (Δf_D) that falls within the bandwidth of the lock-in amplifier (125 kHz, Stanford Research SR 810) used for our experiments. Any shift of the dual-comb beat note will induce a shift of Δf_D. We then used a narrow filter (bandwidth 0.3 Hz) on the lock-in amplifier to lock and amplify only the amplitude at 55 Hz. Since the 50 kHz Δf_D beat note has a linewidth of 10 Hz (defined by the spectral linewidth of the dual Stokes soliton beating) with an electrical intensity 1 mV, the frequency shift dependent amplitude change reaches 0.1 mV/Hz in sech^2 approximation. Such intensity variation could be further amplified by 30 dB. Considering that the resolution of the oscilloscope used for our measurements (see Supplementary Fig. S7) is 0.01 mV, we obtain a theoretically maximum resolution of 10^{-4} Hz. More details on the experimental implementation are shown in Supplementary Fig. S7.

Finally, we inject 0.08 pM NH_3 into the chamber (corresponding to concentration of 0.01 pM/L in chamber) and we measure the dual-comb response (**Fig. 4b**). Following interaction between the graphene flake and NH_3, the lock-in amplified intensity increases from 0 to 34 mV on a time-scale of approximately 100 ms, defined by the gas diffusion process in vacuum. When we zoom-in the gas response trace of **Fig. 4b**, we observe clear steps caused by individual molecule adsorption/desorption (**Fig. 4c**). Before injecting the NH_3 gas, the trace is uniformly flat and there is no evidence of any molecular on/off case (state i). Once the NH_3 gas is injected in the chamber, we observe that the intensity curve increases in small steps, suggesting that adsorption of individual molecules occurs (state ii). When the interaction

between the graphene and the NH_3 gas reaches the dynamic balance, the intensity curve becomes flat again, although we can still observe on/off steps due to microscopic molecular thermal motion. **Fig. 4d** shows that the height of all the observed steps are multiple integers of 0.2 mV, which is the smallest number corresponding to individual molecule adsorption. This is another strong evidence that individual molecule dynamics can be detected with our device. We also count the molecular on-off cases occurring within 200 ms after the injection of the gas in the chamber. Gas adsorption dominates during the state ii, and the on-off cases are balanced in the state iii. Moreover, when the GMDC is exposed to NH_3, the large steps are rare (such as > 2 molecular on/off events), whereas unit steps are dominant. These statistical results obey a power-law distribution, which is also a sign of individual molecule adsorption events [10].

To conclude, dual-comb spectroscopy is demonstrated in a graphene functionalized over-modal microresonator. Stokes soliton combs with $\approx$ 1670 nm central wavelength in distinct mode families are co-generated and trapped by the Kerr soliton in the communication band. By placing graphene away from the equator of the microresonator, we managed to simultaneously generate one Stokes soliton interacting with graphene and another Stokes soliton interacting only with the pristine cavity. The former is used as a probe and the latter as a reference for gas sensing. To this end, we measured the probe-reference intermode dual-comb beating signal in the in the RF spectral region and thanks to a heterodyne lock-in scheme we achieved sub Hz spectral resolution and individual molecule sensitivity. This scheme offers a label-free optical tool to realize individual gas molecule detection. Such a compact device not only demonstrates a unique potential for chemical sensing, but also paves the way to design novel microcomb devices for applications ranging from radio signal generators, frequency modulators and to spatial rangefinders.

Methods

Co-generation of the Kerr and Stokes solitons. The Kerr comb generation relies on phase-matched four-wave-mixing, while Stokes comb excitation is based on the Raman gain. The photonic energy transfers from the pumping laser and the Kerr comb (C band) to the Stokes lines (U band). Once the laser pump detuning > 5 GHz, the excitation of Stokes combs appear in distinct mode families. 1) By using the finite-element-method, we analyze the mode distributions and refractive indices in the microsphere, and discuss the influence for Kerr-Stokes comb interaction. 2) By using the Lugiato-Lefever-equation with a Raman term, we theoretically analyze the comb formation and trapping and investigate the temporal and spectral evolutions numerically. A detailed discussion is shown in Supplementary Note S1 and S2.

Fabrication of the graphene deposited microspheres. We fabricate the microsphere resonators based on electrical arc discharging thermal melting-shaping technique, which is implemented in a high power fiber fusion splicer (FITEL S184; FITEL S178). By controlling the arc discharge power, discharge duration and discharge position, we can control the diameter of the microspheres. Here we use $\approx$ 620 μm diameter microspheres because they can support hundreds of transverse mode families. For soliton comb formation, these samples can produce a repetition rate $\approx$ 100 GHz. The arc-melting-shaping scheme ensures the surface uniformity and smoothness, enabling ultrahigh Q factor (>10^8) for light oscillation.

Afterwards, we prepare the high-quality crystalline graphene via PDMS based mechanical exfoliation. Then, by using the dry-transfer technique, we deposit the graphene nano-layer on the surface of the microsphere. In this implementation, we carefully optimize the graphene location, making sure that some modes of the intracavity transmitting light can interact with the graphene, while the graphene is not at the equator of the microresonator. The fabrication steps and characterization of the device are shown in Supplementary Note S3.

Experimental setups. We check the transmission of our cavities and the Q factor of the resonators by sweeping the ECDL wavelength 1550 nm to 1551 nm, fixing the ECDL power at 0.2 mW to avoid any ringdown. The tunable laser is connected to an oscilloscope to provide a trigger for time-frequency calibration. The spectral sampling rate can be as low as 1 kHz, which allows to identify resonances in the MHz level. The Q factor corresponds to the carrier frequency times the width of the resonance. For soliton comb formation, we use the power kicking scheme, via detuning the C-band tunable laser diode into the resonances, after erbium based amplification (pumping power 120 mW). Light is launched in and collected by using a tapered fiber with diameter 1 μm. We use a commercial frequency resolved optical gating (FROG, MesoPhotonics) to measure the pulse durations and the high repetition rates. This contains a motor controlled tunable mechanical travel stage, a BBO crystal to generate SHG, and a visible band OSA (ocean optics) for spectral analysis, with spectral resolution 0.2 nm, measurement window 20 ps, and sampling rate 10 fs/point. To achieve the SHG threshold, the average comb power is amplified to 1 W. For the optoelectronic sensitivity enhancement, we first use an amplified photodetector (PD, Thorlabs APD 103C) to extract the dual-comb beat note. Then a wave generator (Tektronix AFG 3100, 250 MHz) is used to produce an electric signal for further down conversion of the comb beat note to 50 kHz. Finally, we use a lock-in amplifier to complete the heterodyne measurement. More details are shown in Supplementary Note S4-S7.

Declarations

Author contributions. B.Y. and Y.R. led this work. Z.Y., T.T., G.Y. and B.Y. performed the optical measurements. Z.Y. and T.T. fabricated the silica microspheres. Z.Y., S.Z., H.Z. and B.P. performed the graphene deposition and characterization. G.S. and B.Y. performed the theoretical analysis of the graphene optoelectronics. B.Y., Z.Y. and T.T. contributed the principal investigations of the Kerr-Raman soliton generation spectroscopy. N.A., Z.Y., G.Y. and T.T. performed the ultrafast identification and heterodyne measurement. Z.Y., T.T. and N.A. performed the gas sensing measurements. All the authors discussed and analyzed the results. B.Y., G.S. and Y.R. prepared the manuscript.

**Competing interests.** The authors declare no competing financial interests.

Data availability. The data that support the plots and maps within this paper and other findings of this study are available from the corresponding authors upon reasonable request.

References

1. Picqué, N. & Hänsch, T. W. Frequency comb spectroscopy. *Nat. Photonics* **13**, 146–157 (2019).

2. Coddington, I., Newbury, N. & Swann, W. Dual-comb spectroscopy. *Optica* **3**, 414 (2016).

3. Suh, M.-G., Yang, Q.-F., Yang, K. Y., Yi, X. & Vahala, K. J. Microresonator soliton dual-comb spectroscopy. *Science* **354**, 600–603 (2016).

4. Link, S. M., Maas, D. J. H. C., Waldburger, D. & Keller, U. Dual-comb spectroscopy of water vapor with a free-running semiconductor disk laser. *Science* **356**, 1164–1168 (2017).

5. Yu, M. *et al.* Silicon-chip-based mid-infrared dual-comb spectroscopy. *Nat. Commun.* **9**, 1869 (2018).

6. Bao, C., Suh, M.-G. & Vahala, K. Microresonator soliton dual-comb imaging. *Optica* **6**, 1110 (2019).

7. Lucas, E. *et al.* Spatial multiplexing of soliton microcombs. *Nat. Photonics* **12**, 699–705 (2018).

8. Yang, Q.-F., Yi, X., Yang, K. Y. & Vahala, K. Stokes solitons in optical microcavities. *Nat. Phys.* **13**, 53–57 (2017).

9. Cao, Z. *et al.* Biochemical sensing in graphene-enhanced microfiber resonators with individual molecule sensitivity and selectivity. *Light Sci. Appl.* **8**, 107 (2019).

10. An, N. *et al.* Electrically Tunable Four-Wave-Mixing in Graphene Heterogeneous Fiber for Individual Gas Molecule Detection. *Nano Lett.* **20**, 6473–6480 (2020).

11. Heylman, K. D. *et al.* Optical microresonators as single-particle absorption spectrometers. *Nat. Photonics* **10**, 788–795 (2016).

12. Mauranyapin, N. P., Madsen, L. S., Taylor, M. A., Waleed, M. & Bowen, W. P. Evanescent single-molecule biosensing with quantum-limited precision. *Nat. Photonics* **11**, 477–481 (2017).

13. Rodrigo, D. *et al.* Mid-infrared plasmonic biosensing with graphene. *Science* **349**, 165–168 (2015).

14. Arroyo, J. O. & Kukura, P. Non-fluorescent schemes for single-molecule detection, imaging and spectroscopy. *Nat. Photonics* **10**, 11–17 (2016).

15. Liebel, M., Toninelli, C. & van Hulst, N. F. Room-temperature ultrafast nonlinear spectroscopy of a single molecule. *Nat. Photonics* **12**, 45–49 (2018).

16. Chen, W., Özdemir, Ş. K., Zhao, G., Wiersig, J. & Yang, L. Exceptional points enhance sensing in an optical microcavity. *Nature* **548**, 192–195 (2017).

17. Hodaei, H. *et al.* Enhanced sensitivity at higher-order exceptional points. *Nature* **548**, 187–191 (2017).

18. Kippenberg, T. J., Gaeta, A. L., Lipson, M. & Gorodetsky, M. L. Dissipative Kerr solitons in optical microresonators. *Science* **361**, eaan8083 (2018).

19. Yao, B. *et al.* Gate-tunable frequency combs in graphene–nitride microresonators. *Nature* **558**, 410–414 (2018).

20. Phare, C. T., Daniel Lee, Y.-H., Cardenas, J. & Lipson, M. Graphene electro-optic modulator with 30 GHz bandwidth. *Nat. Photonics* **9**, 511–514 (2015).

21. Datta, I. *et al.* Low-loss composite photonic platform based on 2D semiconductor monolayers. *Nat. Photonics* **14**, 256–262 (2020).

22. Qin, C. *et al.* Electrically controllable laser frequency combs in graphene-fibre microresonators. *Light Sci. Appl.* **9**, 185 (2020).

23. Schedin, F. *et al.* Detection of individual gas molecules adsorbed on graphene. *Nat. Mater.* **6**, 652–655 (2007).

24. Liu, Y., Huang, Y. & Duan, X. Van der Waals integration before and beyond two-dimensional materials. *Nature* **567**, 323–333 (2019).

25. Jia, K. *et al.* Photonic Flywheel in a Monolithic Fiber Resonator. *Phys. Rev. Lett.* **125**, 143902 (2020).

26. Huang, S.-W. *et al.* A broadband chip-scale optical frequency synthesizer at 2.7 x 10-16 relative uncertainty. *Sci. Adv.* **2**, e1501489–e1501489 (2016).

27. Das, A. *et al.* Monitoring dopants by Raman scattering in an electrochemically top-gated graphene transistor. *Nat. Nanotechnol.* **3**, 210–215 (2008).

28. Mikhailov, S. A. & Ziegler, K. New electromagnetic mode in graphene. *Phys. Rev. Lett.* **99**, 016803 (2007).

29. Tan, T., Jiang, X., Wang, C., Yao, B. & Zhang, H. 2D Material Optoelectronics for Information Functional Device Applications: Status and Challenges. *Adv. Sci.* **7**, 2000058 (2020).
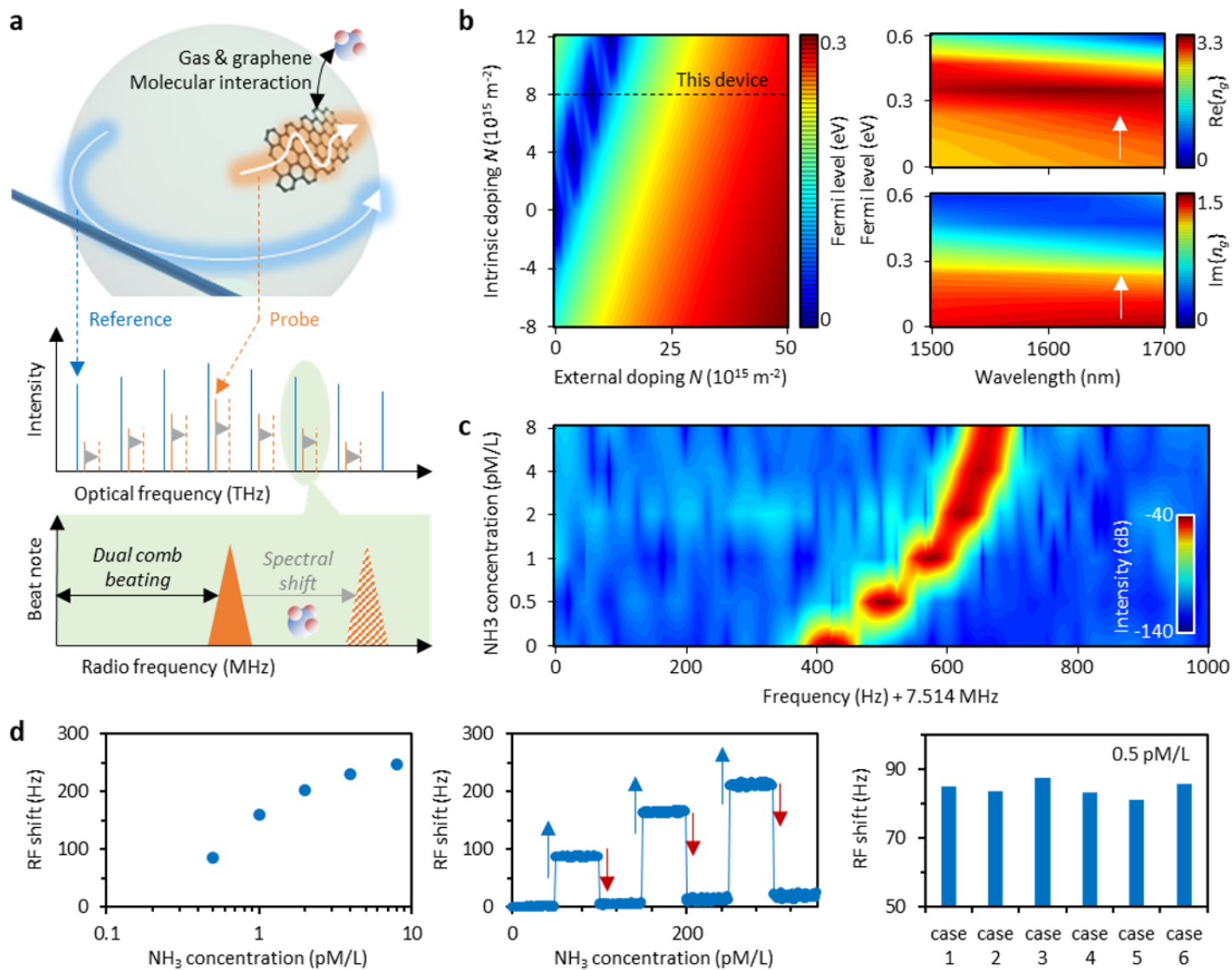
Figures
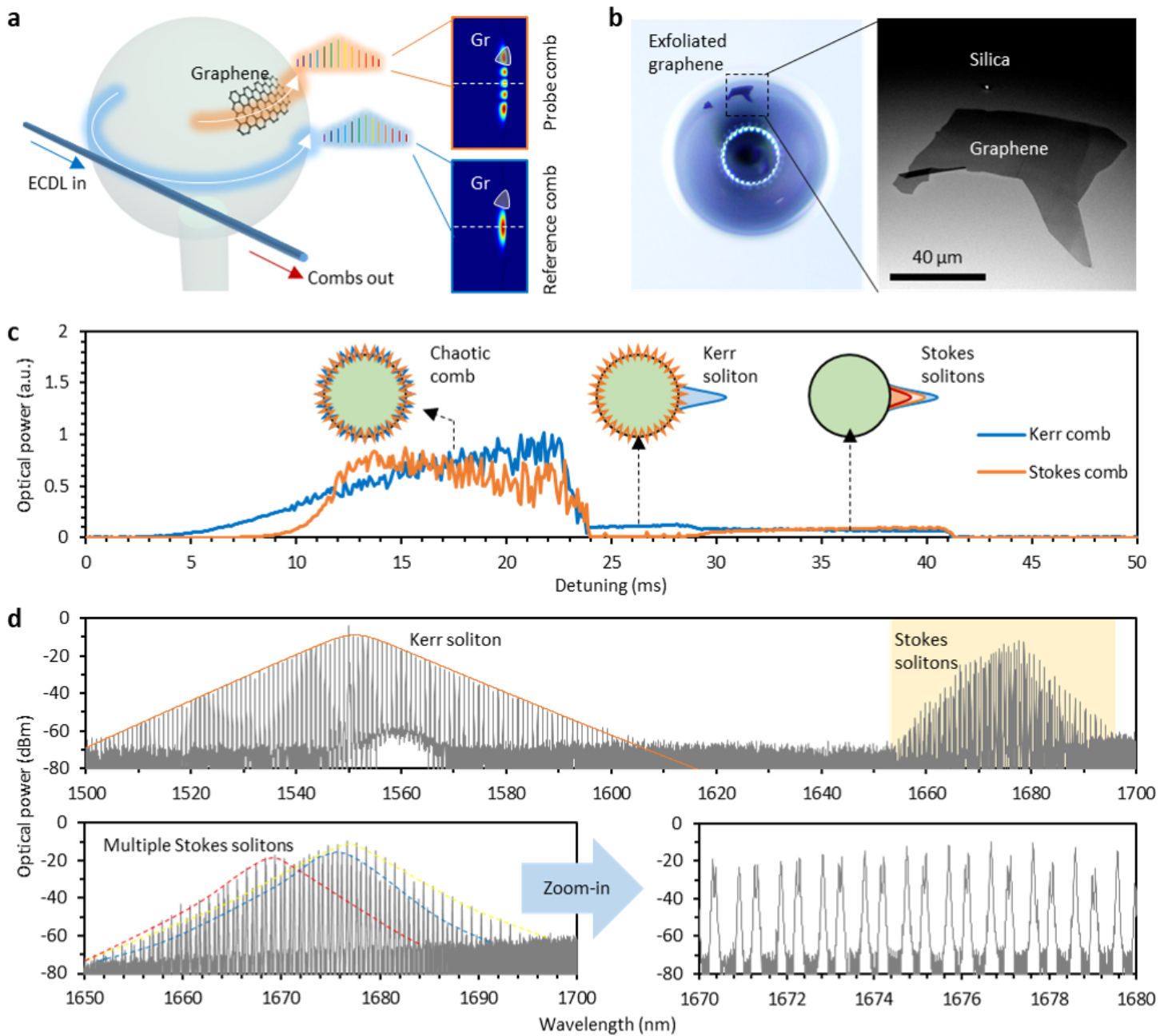
Figure 1

Conceptual design of the graphene based over-modal microresonator and the Kerr-Stokes multiple comb co-generation. a, Schematic diagram of the device. An external cavity diode laser (ECDL) is used as the pump to excite soliton combs, which belong to distinct mode families. Graphene can only influence the comb modes with large spatial distributions. b, The optical microscopy and SEM pictures show the exfoliated graphene deposited on the microsphere, with area ≈ 80 μm × 30 μm. Scale bar: 40 μm. c, Evolution of the Kerr (blue curve) and the Stokes (red curve) combs. d, The measured optical spectrum shows both Kerr soliton and Stokes solitons. The Kerr comb is in the C+L band, and the Stokes comb excited by the Raman gain appear in U band.
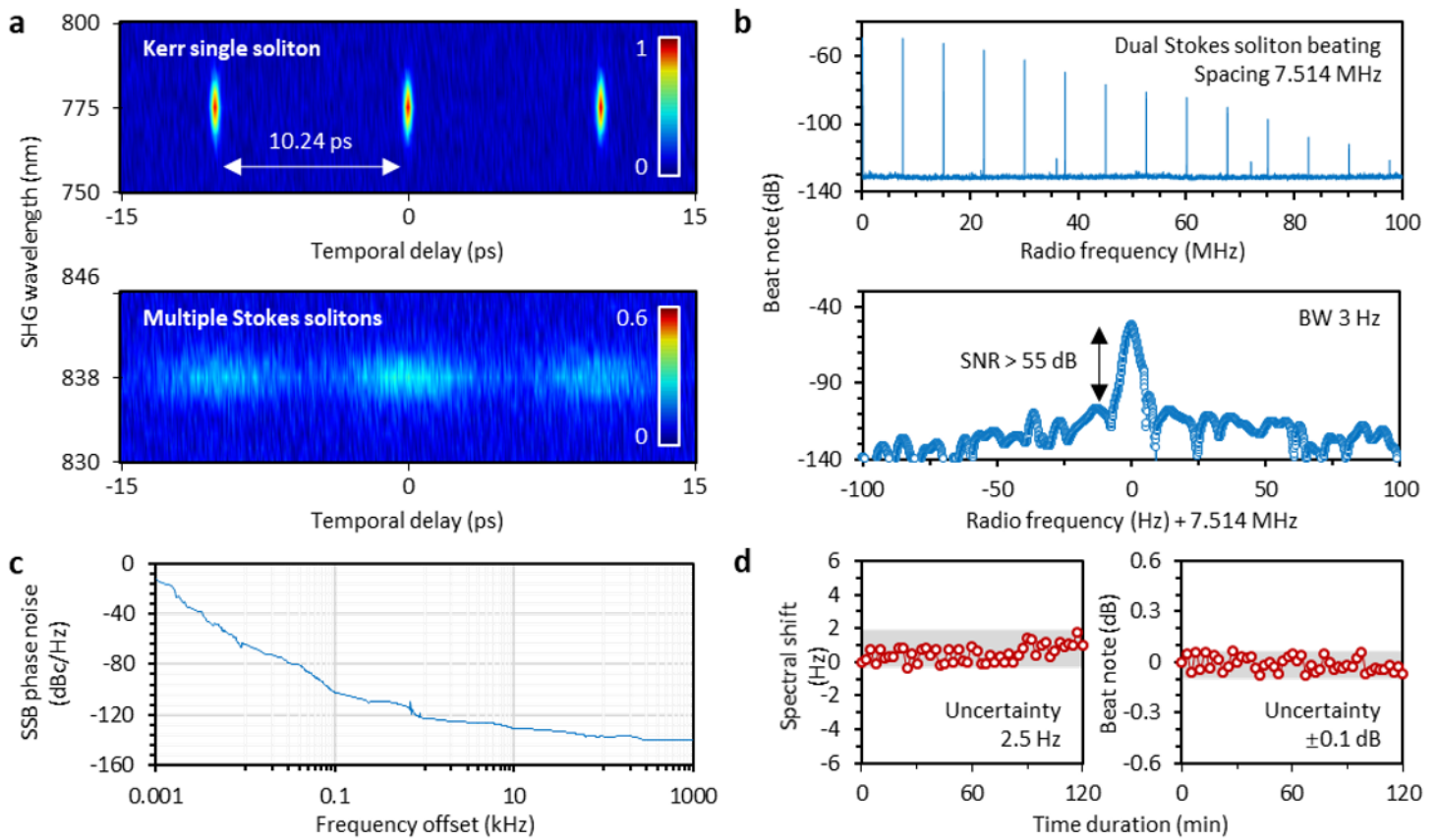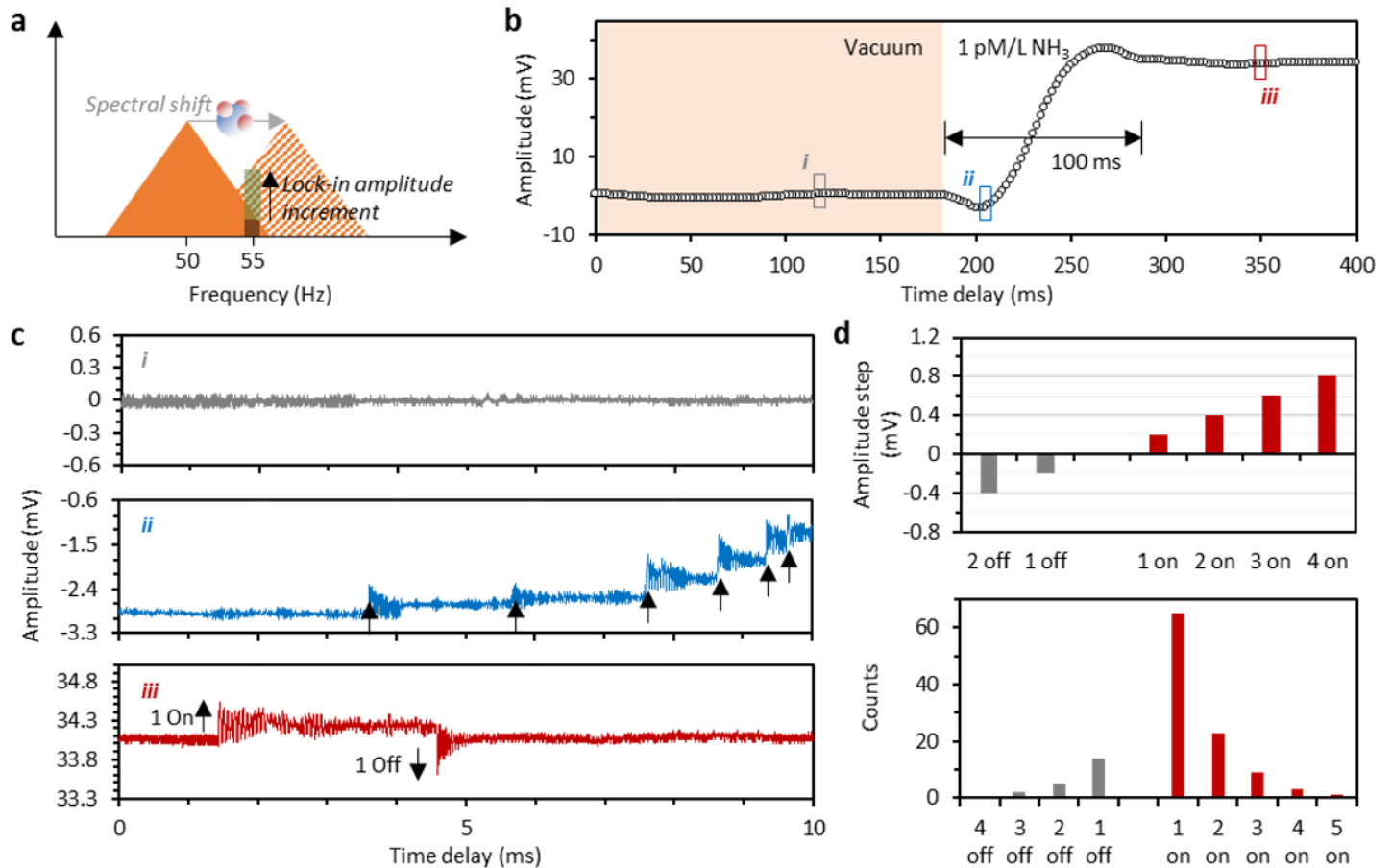
Figure 2

Characterization of the Kerr and Stokes solitons. a, Frequency-resolved auto-correlation maps of the Kerr soliton (top panel) and the Stokes solitons (bottom panel). The color bar shows the normalized intensity of the autocorrelation traces. b, Beat note of the dual Stokes combs in the U band, with 7.514 MHz FSR difference. This shows > 55 dB SNR and < 10 Hz electrical linewidth. c, SSB phase noise down to -140 dBc/Hz of the 7.514 MHz beat note. d, This beat note also displays long-term (>2 hours) stability, with spectral uncertainty < 2.5 Hz, and intensity uncertainty < ±0.1 dB.

Figure 3

Mechanism and performance of the gas sensing device. a, Schematic illustration of the gas sensing device: gas adsorption on the graphene flake changes the comb spacing of the probe soliton, leading to a frequency shift of the dual-comb beat note. b, Simulations show that the gas adsorption changes the EF of graphene and thus modifies the refractive index of the microcavity. Here the white arrows marks the central wavelength of the Stokes comb. c, Measured frequency shift of the dual-comb beat note with initial frequency 7.514 MHz. In this measurement, gas concentration is tuned at 0.5 pM/L, 1 pM/L, 2 pM/L, 4 pM/L, and 8 pM/L. d, Left: correlation of the frequency shift and the gas concentration; Middle: the recovery capability (blue arrows: gas in, red arrows: gas release from graphene); Right: repeated measurement showing that the maximum sensitivity for 0.5 pM/L NH3 is 170 Hz/(pM/L) on average.

Figure 4

Detection of individual molecule dynamics. a, Principle of the lock-in amplification for enhanced individual molecule detection. This technique enables us to detect a small frequency shift ($\approx$ Hz) as a large (> 30dB) change in intensity. b, Measured output trace of the lock-in amplifier, the amplitude increment is induced by the gas absorption on graphene. After injection of the gas in the chamber, the time window to switch from state i (vaccum) to state iii (dynamic balance) is $\approx$ 100 ms. c, Zoomed-in panels of b. Discrete steps in state ii and iii suggest individual molecule on/off events. d, Top panel: the measured steps are integer multiples of 0.2 mV. Bottom panel: We count the molecular on/off (adsorption/desorption) events. The obtained statistics follow a power law.

Supplementary Files

This is a list of supplementary files associated with this preprint. Click to download.

- 003supplementary.docx